On the Channel Quality of XL-MIMO Systems

Yuhao Zhu, Zheng Wang, Yong Zeng, Yongming Huang
School of Information Science and Engineering,
Southeast University, Nanjing, China
Email: {yh.zhu, zheng_wang, yong_zeng, huangym}@seu.edu.cn

***Abstract*—Low-complexity schemes have been widely applied in massive MIMO systems to alleviate the complexity burden associated with high-dimensional signal processing. However, in XL-MIMO systems, many traditional low-complexity methods become impractical due to the significant degradation of channel conditions caused by near-field effects. In this paper, we propose the diagonal dominance ratio indicator (DDRI) of the Gram matrix to effectively assess the channel quality in XL-MIMO systems. Building upon this metric, conventional low-complexity schemes can be adaptively selected and reliably deployed for efficient implementation. Specifically, we first derive a closed-form expression for this metric under LoS conditions, and extend the analysis to NLoS conditions through the random matrix theory. Then, according to the derived results, we obtain a closed-form approximation of the proposed DDRI that admits $\mathcal{O}(1)$ complexity, enabling efficient evaluation of channel quality. Simulation results validate the theoretical analysis and demonstrate the effectiveness of the proposed metric.**

***Index Terms*—Extremely large-scale MIMO, diagonal dominance, channel quality, low-complexity signal processing.**

I. Introduction

To meet the stringent performance requirements of 6G networks, recent advancements have introduced extremely large-scale MIMO (XL-MIMO) systems, which deploy much more antennas compared to conventional massive MIMO systems [1]. However, as the array aperture expands, communication distances now fall within the near-field Rayleigh region. Therefore, the channel modeling paradigm shifts from the uniform plane wave (UPW) approximation to the non-uniform spherical wave (NUSW) model exhibiting pronounced spatial non-stationarity [2] [3]. Unfortunately, this change may lead to an ill-conditioned channel, which is substantially different from the favorable channel condition in massive MIMO.

Specifically, conventional far-field massive MIMO systems benefit from channel hardening and favorable propagation, where the channel matrix becomes near-orthogonal as the number of BS antennas increases. Leveraging this property, numerous low-complexity methods have been developed to achieve near-optimal performance while bypassing complicated matrix computations, including approximate inversion techniques [4] and iterative solvers [5]. However, these methods are highly sensitive to channel conditions and experience slow convergence and diminished accuracy once channel conditions deteriorate. As a result, they may not be well suited to XL-MIMO systems, where the channel conditions are more challenging.

Corresponding author: Zheng Wang (email: wznuaa@gmail.com)

In this paper, we propose an effective yet computationally efficient metric, the Gram matrix diagonal dominance ratio indicator (DDRI), for assessing XL-MIMO channel quality. Rather than universally resorting to high-complexity processing, our approach leverages DDRI to evaluate the channel quality with minimal computational overhead. In particular, a closed-form approximation of the proposed DDRI is derived in terms of the UE and BS geometric parameters (i.e., the link distance and angles), which enables $\mathcal{O}(1)$ complexity without explicitly forming the Gram matrix. Based on it, transceivers can adaptively select the appropriate signal processing strategy that best suits the current channel conditions. Overall, our methods enable the avoidance of unnecessary computational expenditure, achieving significant complexity reduction with negligible performance loss.

II. Preliminary

Consider a near-field XL-MIMO communication system illustrated in Fig. 1, where the BS and the UE employ uniform linear arrays (ULAs) with N and K antenna elements, respectively. The inter-element spacings are d_r (BS) and d_t (UE). The BS array lies in the xy-plane, is centered at the origin, and its axis is oriented by the azimuth angle θ_r, yielding the unit direction vector $\mathbf{u}_r = [\sin\theta_r, \cos\theta_r, 0]^T$. Without loss of generality, the UE array center is placed at $\mathbf{c}_t = [r_0, 0, 0]^T$, and its axis is oriented by elevation θ_t and azimuth φ_t, with unit direction vector $\mathbf{u}_t = [\sin\theta_t\cos\varphi_t, \cos\theta_t, \sin\theta_t\sin\varphi_t]^T$. Let $n \in \mathcal{I}_N = \{-(N-1)/2, \ldots, (N-1)/2\}$ and $k \in \mathcal{I}_K = \{-(K-1)/2, \ldots, (K-1)/2\}$ index BS and UE elements, respectively. The element positions are $\mathbf{b}_n = nd_r\mathbf{u}_r$ and $\mathbf{t}_k = \mathbf{c}_t + kd_t\mathbf{u}_t$.

For XL-MIMO system, the received signal vector $\mathbf{y} \in \mathbb{C}^N$ can be expressed as

$$\mathbf{y} = \mathbf{H}\mathbf{x} + \mathbf{n}, \tag{1}$$

where $\mathbf{x} \in \mathbb{C}^K$ is the transmitted symbol vector with covariance $\mathbb{E}\{\mathbf{x}\mathbf{x}^H\} = \mathbf{I}_K$, and $\mathbf{n} \in \mathbb{C}^N$ is additive white Gaussian noise (AWGN) satisfying zero mean and $\mathbb{E}\{\mathbf{n}\mathbf{n}^H\} = \sigma_n^2\mathbf{I}_N$.

The near-field channel matrix $\mathbf{H} \in \mathbb{C}^{N\times K}$ is composed of both LoS and NLoS components [6]

$$\mathbf{H} = \sqrt{\frac{\kappa}{\kappa+1}}\,\mathbf{H}_{\mathrm{LoS}} + \sqrt{\frac{1}{\kappa+1}}\,\mathbf{H}_{\mathrm{NLoS}}, \tag{2}$$

where κ is the Rician K-factor, representing the relative power between the LoS and NLoS components. Under spherical-wave

$$r_{n,k} = \sqrt{[r_0 + kd_t \sin\theta_t \cos\varphi_t - nd_r \sin\theta_r]^2 + [kd_t \sin\theta_t \sin\varphi_t]^2 + [kd_t \cos\theta_t - nd_r \cos\theta_r]^2}$$
$$\approx r_0 + (-nd_r \sin\theta_{\rm r} + \tfrac{(nd_r \cos\theta_{\rm r})^2}{2r_0}) + (kd_t \sin\theta_{\rm t} \cos\varphi_{\rm t} + \tfrac{(kd_t \sin\theta_{\rm t} \sin\varphi_{\rm t})^2}{2r_0} + \tfrac{(kd_t \cos\theta_{\rm t})^2}{2r_0}) - \tfrac{d_t d_r\, nk \cos\theta_{\rm t} \cos\theta_{\rm r}}{r_0} \tag{5.b}$$

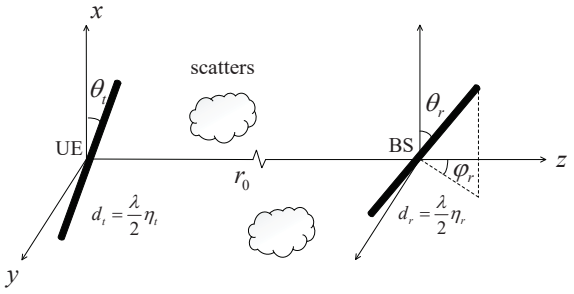

Fig. 1. Overview of near-field XL-MIMO configuration with dual-ULAs.

propagation, the deterministic LoS component between BS element n and UE element k is

$$[\mathbf{H}_{\rm LoS}]_{n,k} = \frac{\rho}{r_{n,k}} \exp\left(-{\rm j}\frac{2\pi}{\lambda} r_{n,k}\right), \tag{3}$$

where ρ is the small scale channel gain and $r_{n,k}$ is the distance between two antennas. Meanwhile, the NLoS component is modeled as independent but not identically distributed complex Gaussian fading with distance-dependent variance

$$[\mathbf{H}_{\rm NLoS}]_{n,k} \sim \frac{\rho}{r_{n,k}} \mathcal{CN}(0,1). \tag{4}$$

Here, $r_{n,k}$ denotes the propagation distance between the n-th element of BS and the k-th element of UE, i.e., $r_{n,k} = \|\mathbf{b}_n - \mathbf{t}_k\|$. Note that in this paper the case that the array aperture is much smaller than the link distance is considered, which is widely applied in the model of XL-MIMO systems [7]. In this condition, the amplitude variations across the array are negligible and absorbed into a constant gain, i.e.,

$$\tilde{\beta} \triangleq \rho / r_0 \tag{5.a}$$

While the phase requires a more accurate Fresnel approximation due to its sensitivity to the inter-element path-length differences [1]. To be specific, the exact expression of $r_{n,k}$ and its corresponding approximation are given in (5.b).

To characterize the channel quality, the effective degrees of freedom (EDoF) is a commonly used metric that reflects the number of substreams channel can support, defined as

$$\varepsilon = \left(\frac{{\rm Tr}(\mathbf{G})}{\|\mathbf{G}\|_F}\right)^2 = \frac{(\sum_i \lambda_i)^2}{\sum_i \lambda_i^2}, \tag{6}$$

where $\mathbf{G} = \mathbf{H}^H\mathbf{H}$ is the Gram matrix representing the correlation of the channel matrix, and λ_i denotes the i-th largest eigenvalues of $\mathbf{G}$. Typically, a higher value of EDoF corresponds to a better-conditioned channel with lower correlation. However, the main limitation of EDoF is its prohibitive computational cost, as it requires the full set of singular values. This operation has a complexity of $\mathcal{O}(NK^2)$, making it impractical for real-time channel assessment, especially in large-scale systems.

III. Diagonal Dominance Ratio Indicator of Gram Matrix

With respect to the Gram matrix $\mathbf{G} = \mathbf{H}^H\mathbf{H}$, its diagonal ratio is considered as

$$\alpha_i = \frac{|g_{ii}|}{\sum_{j=1}^K |g_{ij}|} = \frac{|g_{ii}|}{|g_{ii}| + \sum_{j\neq i} |g_{ij}|} \tag{7}$$

for the i-th stream, where $g_{ij} = \mathbf{h}_i^H \mathbf{h}_j$ is the (i,j)-th entry of $\mathbf{G}$. Typically, α_i quantifies the ratio of desired signal power to total signal and inter-stream interference. Based on α_i, to better evaluate the channel quality of $\mathbf{H}$, we now define the Gram matrix diagonal dominance ratio indicator (DDRI) as

$$\alpha^* \triangleq \min_{1\leq i\leq K} \alpha_i, \tag{8}$$

and it is natural to deduce that a larger α^* implies stronger diagonal dominance of $\mathbf{G}$. In particular, when $\alpha^* \geq 1/2$, $\mathbf{G}$ is diagonal dominant by satisfying [4]

$$|g_{ii}| \geq \sum_{j\neq i} |g_{ij}|, \quad \forall i = 1,2,...,K. \tag{9}$$

Put it another way, this implies that the channel matrix $\mathbf{H}$ is near orthogonal with a good channel condition, which can be verified by the following result.

Corollary 1. *When $\alpha^* \geq 1/2$, the condition number of $\mathbf{H}$ is upper bounded by*

$${\rm cond}(\mathbf{H}) \leq \sqrt{\frac{g_{\max}}{g_{\min}} \frac{1}{2\alpha^* - 1}}, \tag{10}$$

where $g_{\max}$ and $g_{\min}$ are the maximum and minimum value of diagonal entries of $\mathbf{G}$.

Proof: Let $G_i = \sum_{j\neq i} |g_{ij}|$ denote the absolute row sums of the i-th row without the diagonal element. Since $\mathbf{G}$ is Hermitian, Gershgorin's disk theorem reduces to intervals on the real axis. Therefore, the eigenvalues of $\mathbf{G}$ satisfy [8]

$$\min_i (g_{ii} - G_i) \leq \lambda_i(\mathbf{G}) \leq \max_i (g_{ii} + G_i). \tag{11}$$

After that, substituting $G_i = (1/\alpha_i - 1)g_{ii}$ into (11) yields the following bounds on the extreme eigenvalues

$$\min_i(g_{ii}(2 - 1/\alpha_i)) \leq \lambda_{\min}(\mathbf{G}) \leq \lambda_{\max}(\mathbf{G}) \leq \max_i(g_{ii}/\alpha_i). \tag{12}$$

Finally, recalling that ${\rm cond}(\mathbf{H}) = \sqrt{\lambda_{\max}/\lambda_{\min}}$ completes the proof. ■

Based on Corollary 1, the channel condition of $\mathbf{H}$ can be well evaluated by the proposed DDRI α^*.

For a better understanding, Fig. 2 is provided to illustrate the relationship between DDRI and the condition number of

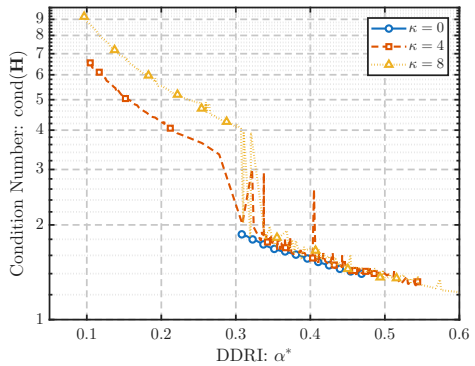

Fig. 2. Relationship between DDRI α^* and the condition number $\mathrm{cond}(\mathbf{H})$ for the near-field channel model in (2).

$\mathbf{H}$, where $\mathrm{cond}(\mathbf{H})$ monotonically decreases with the improvement of α^*. Motivated by this, we further propose applying $\alpha^* \geq 1/2$ as a decision threshold to select the upcoming signal processing solutions.

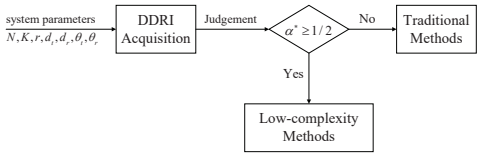

Fig. 3. The structure of the proposed DDRI-based judgement mechanism

Specifically, as shown in Fig. 3, when $\alpha^* \geq 1/2$, by Corollary 1, the channel is deemed as well-conditioned such that the traditional low-complexity schemes can be employed as usual. Otherwise, the channel turns out to be ill-conditioned. To be more specific, the columns of $\mathbf{H}$ are highly correlated with each other, such that those traditional low-complexity schemes that chiefly depend on good channel conditions may fail to work. Hence, in this condition, the classic signal processing solutions are preferred for the sake of system performance. Overall, thanks to this judgement mechanism, low-complexity schemes can be reasonably applied to XL-MIMO systems with negligible performance loss. Nevertheless, we have to point out that the key to such a mechanism heavily lies in efficiently computing the proposed DDRI α^*, which will be fully investigated in the following section.

IV. Efficient Approximation of DDRI

Regarding the channel matrix $\mathbf{H}$, in order to efficiently obtain its DDRI α^*, we first decompose the Gram matrix $\mathbf{G} = \mathbf{H}^H\mathbf{H}$ based on the channel model in (2), i.e.,

$$\begin{aligned}\mathbf{G} = &\frac{\kappa}{\kappa+1}\mathbf{H}_{\mathrm{LoS}}^H\mathbf{H}_{\mathrm{LoS}} + \frac{1}{\kappa+1}\mathbf{H}_{\mathrm{NLoS}}^H\mathbf{H}_{\mathrm{NLoS}} \\ &+ \frac{\sqrt{\kappa}}{\kappa+1}(\mathbf{H}_{\mathrm{LoS}}^H\mathbf{H}_{\mathrm{NLoS}} + \mathbf{H}_{\mathrm{NLoS}}^H\mathbf{H}_{\mathrm{LoS}}).\end{aligned} \tag{13}$$

Since $\mathbf{H}_{\mathrm{LoS}}$ is deterministic and $\mathbf{H}_{\mathrm{NLoS}}$ is statistical with zero mean, the cross terms in (13) (i.e., $\mathbf{H}_{\mathrm{LoS}}^H\mathbf{H}_{\mathrm{NLoS}}$ and $\mathbf{H}_{\mathrm{NLoS}}^H\mathbf{H}_{\mathrm{LoS}}$) would vanish in terms of expectation, so as to

$$\mathbb{E}[\mathbf{G}] = \frac{\kappa}{\kappa+1}\mathbf{G}_{\mathrm{LoS}} + \frac{1}{\kappa+1}\mathbb{E}[\mathbf{G}_{\mathrm{NLoS}}]. \tag{14}$$

Then, based on (14), we begin to analyze $\mathbf{G}_{\mathrm{LoS}}$ and $\mathbf{G}_{\mathrm{NLoS}}$, respectively, to seek for the efficient approximation of α^*.

A. Efficient Approximation for Components of $\mathbf{G}_{\mathrm{LoS}}$

We begin with the entrywise analysis of the associated Gram matrix $\mathbf{G}_{\mathrm{LoS}}$. According to (5.a) and (5.b), $\mathbf{H}_{\mathrm{LoS}}$ can be factorized by

$$\mathbf{H}_{\mathrm{LoS}} = \tilde{\beta}\,\mathbf{\Phi}_r\mathbf{V}\mathbf{\Phi}_t^H e^{-\mathrm{j}2\pi r_0/\lambda}, \tag{15}$$

where $\mathbf{\Phi}_r \in \mathbb{C}^{N\times N}$ and $\mathbf{\Phi}_t \in \mathbb{C}^{K\times K}$ are diagonal and unitary matrices accounting for the phase shifts induced by BS and UE, respectively, and $\mathbf{V} \in \mathbb{C}^{N\times K}$ is a Vandermonde matrix accounting for the array coupling. Specifically, the entries in $\mathbf{\Phi}_r$ $\mathbf{\Phi}_t$ and $\mathbf{V}$ are given by

$$[\mathbf{\Phi}_r]_{n,n} = \exp\left[\mathrm{j}\tfrac{2\pi n d_r \sin\theta_r}{\lambda} - \mathrm{j}\tfrac{\pi(n d_r\cos\theta_r)^2}{\lambda r_0}\right], \tag{16}$$

$$\begin{aligned}[\mathbf{\Phi}_t]_{k,k} = \exp\Big[&\mathrm{j}\tfrac{2\pi k d_t \sin\theta_t\cos\varphi_t}{\lambda} - \mathrm{j}\tfrac{\pi}{\lambda r_0}\big((k d_t\sin\theta_t\sin\varphi_t)^2 \\ &+ (k d_t\cos\theta_t)^2\big)\Big],\end{aligned} \tag{17}$$

$$[\mathbf{V}]_{n,k} = \exp\left[\mathrm{j}\,\frac{2\pi d_t d_r\cos\theta_t\cos\theta_r}{\lambda r_0} nk\right] \triangleq \exp\left(\mathrm{j}2\eta nk\right). \tag{18}$$

Here, we introduce a near-field coupling parameter as follows

$$\eta \triangleq \pi d_t d_r\cos\theta_t\cos\theta_r/(\lambda r_0). \tag{19}$$

Note that this parameter bears the information of array spacing d_t, d_r and link distance r_0.

Then, based on (15), $\mathbf{G}_{\mathrm{LoS}}$ can be expressed as,

$$\begin{aligned}\mathbf{G}_{\mathrm{LoS}} &= \tilde{\beta}^2[\mathbf{\Phi}_r\mathbf{V}\mathbf{\Phi}_t^H]^H\mathbf{\Phi}_r\mathbf{V}\mathbf{\Phi}_t^H \\ &\overset{(a)}{=} \tilde{\beta}^2\mathbf{\Phi}_t\mathbf{V}^H\mathbf{V}\mathbf{\Phi}_t^H,\end{aligned} \tag{20}$$

where equality (a) holds because of $\mathbf{\Phi}_r^H\mathbf{\Phi}_r = \mathbf{I}$.

Then, since $\mathbf{\Phi}_t$ is diagonal with unit-modulus entries, left and right multiplication by $\mathbf{\Phi}_t$ preserves the entrywise magnitudes of $\mathbf{G}_{\mathrm{LoS}}$, namely

$$\left|[\mathbf{\Phi}_t\mathbf{V}^H\mathbf{V}\mathbf{\Phi}_t^H]_{i,j}\right| = \left|[\mathbf{V}^H\mathbf{V}]_{i,j}\right|. \tag{21}$$

Hence, the entrywise magnitude of $\mathbf{G}_{\mathrm{LoS}}$ is primarily determined by the scalar factor $\tilde{\beta}^2$ and inner product $\mathbf{V}^H\mathbf{V}$ with

$$[\mathbf{V}^H\mathbf{V}]_{i,j} = \sum_{n=1}^{N} e^{(-\mathrm{j}2\eta n(i-j))} = e^{-\mathrm{j}\eta(i-j)(N+1)}\tfrac{\sin(N\eta(i-j))}{\sin(\eta(i-j))}. \tag{22}$$

Meanwhile, as $[\mathbf{V}^H\mathbf{V}]_{i,j}$ depends solely on the index difference $\delta \triangleq |i-j| = 1, 2, ..., K-1$, the magnitudes of the components in $\mathbf{G}_{\mathrm{LoS}}$ exhibit a Toeplitz structure, such that

$$|g_{ii}^{\mathrm{LoS}}| = \tilde{\beta}^2 N \quad \text{and} \quad |g_{ij}^{\mathrm{LoS}}| = \tilde{\beta}^2\left|\tfrac{\sin(N\eta\delta)}{\sin(\eta\delta)}\right| \text{ for } i \neq j. \tag{23}$$

Lemma 1. *For $N, K \to \infty$ with $K/N < 1$, by defining $G_i^{\mathrm{LoS}} \triangleq \sum_{j\neq i}|g_{ij}^{\mathrm{LoS}}|$, it follows that*

$$G_i^{\mathrm{LoS}} \approx \frac{\tilde{\beta}^2}{\eta}\left(\frac{2}{\pi}\ln(NK\eta) + C\right), \tag{24}$$

where C is a constant independent of N, K and η.

Proof: To begin with, according to (23), the discrete sum in G_i^{LoS} follows

$$\begin{aligned} G_i^{\mathrm{LoS}} &= \tilde{\beta}^2 \sum_{\delta=1}^{K-1} \frac{|\sin(N\eta\delta)|}{|\sin(\eta\delta)|} \overset{(a)}{\approx} \frac{\tilde{\beta}^2}{\eta} \int_0^{K\eta} \frac{|\sin(N\delta)|}{|\sin\delta|} \mathrm{d}\delta \\ &\overset{(b)}{=} \frac{\tilde{\beta}^2}{\eta} \int_0^{NK\eta} \frac{|\sin t|}{|\sin(t/N)|} \frac{\mathrm{d}t}{N} \\ &\overset{(c)}{\approx} \frac{\tilde{\beta}^2}{\eta} \int_0^{NK\eta} \frac{|\sin t|}{t} \mathrm{d}t = \frac{\tilde{\beta}^2}{\eta} J(NK\eta) \end{aligned} \tag{25}$$

with $J(x) \triangleq \int_0^x |\sin t|/t \mathrm{d}t$. Here, (a) approximates the discrete sum by its integral form, (b) applies the substitution $t \triangleq N\delta$, (c) stems from Taylor expansion $\sin(\epsilon) = \epsilon - \epsilon^3/(3!) + \mathcal{O}((\epsilon)^5)$.

Next, with respect to $J(x)$, the integral interval $[0, x]$ can be partitioned into $M = \lfloor x/\pi \rfloor$ main sub-intervals as follows

$$[0, x] = \underbrace{[0, \pi] \cup \ldots \cup [(M-2)\pi, (M-1)\pi)]}_{M \text{ sub-intervals}} \cup \underbrace{[M\pi, x]}_{\text{residual part}}. \tag{26}$$

Based on it, $J(x)$ can be rewritten as follows

$$J(x) = \underbrace{\sum_{k=0}^{M-1} \int_0^{\pi} \frac{\sin t}{t} \mathrm{d}t}_{S(x)} + \underbrace{\int_0^{x-M\pi} \frac{\sin t}{t} \mathrm{d}t}_{R(x)}. \tag{27}$$

In particular, note that the residual term $R(x)$ in (27) satisfies $0 \le R(x) \le \frac{2}{M\pi} = \mathcal{O}(x^{-1})$, rendering it negligible as $x \to \infty$. Therefore, $J(x)$ can be approximated by

$$J(x) = S(x) + \mathcal{O}(x^{-1}) \tag{28}$$

for a large value of x.

As for $S(x)$ in (27), within each sub-interval, local coordinates are introduced via $t = \tau + k\pi$ with $\tau \in (0, \pi)$, such that

$$S(x) = \sum_{k=0}^{M-1} \int_0^{\pi} \frac{\sin \tau}{\tau + k\pi} \mathrm{d}t. \tag{29}$$

For $k \ge 1$, the denominator $\tau + k\pi$ satisfies $k\pi < \tau + k\pi < (k+1)\pi$, so as to

$$\frac{\sin \tau}{(k+1)\pi} < \frac{\sin \tau}{\tau + k\pi} < \frac{\sin \tau}{k\pi} \tag{30}$$

because of $\sin \tau > 0$ in each sub-interval.

Meanwhile, since numerator $\sin \tau$ satisfies $\int_0^{\pi} \sin \tau d\tau = 2$, integrating (30) over $[0, \pi]$ obtains

$$\frac{2}{(k+1)\pi} < \int_0^{\pi} \frac{\sin \tau}{\tau + k\pi} \mathrm{d}\tau < \frac{2}{k\pi}. \tag{31}$$

Then, based on (31), the following results about (29) can be arrived:

$$\mathrm{Si}(\pi) + \frac{2}{\pi} \sum_{k=1}^{M-1} \frac{1}{k+1} < S(x) < \mathrm{Si}(\pi) + \frac{2}{\pi} \sum_{k=1}^{M-1} \frac{1}{k}, \tag{32}$$

where the case $k = 0$ is treated separately and captured by $\int_0^{\pi} \sin \tau / \tau d\tau = \mathrm{Si}(\pi)$.

Furthermore, based on (28), by invoking the classical expansion for the harmonic sums, $\sum_{k=1}^{M-1} \frac{1}{k} = \ln M + \gamma + \mathcal{O}(1/M)$ and recalling that $M = \lfloor x/\pi \rfloor$, we can have

$$J(x) = \frac{2}{\pi} \ln(x) + C + \mathcal{O}(x^{-1}), \tag{33}$$

where the constant term C is bounded by

$$\mathrm{Si}(\pi) + \tfrac{2}{\pi}(\gamma - 1 - \ln \pi) \le C \le \mathrm{Si}(\pi) + \tfrac{2}{\pi}(\gamma - \ln \pi). \tag{34}$$

Finally, matching the integral interval in (25) with $x = NK\eta$ and multiplying by $\tilde{\beta}^2/\eta$, yields the results in (24). ∎

In practice, a larger G_i^{LoS} indicates stronger interference and hence worse channel quality. We therefore adopt the upper bound $C = \mathrm{Si}(\pi) + \frac{2}{\pi}(\gamma - \ln \pi) \approx 1.491$ as a conservative value for the constant C in (24).

B. Efficient Approximation for Components of $\mathbf{G}_{\mathrm{NLoS}}$

Similarly, consider the small aperture assumption in (5.a), $\mathbf{H}_{\mathrm{NLoS}}$ can be expressed by

$$[\mathbf{H}_{\mathrm{NLoS}}]_{n,k} \sim \tilde{\beta} \mathcal{CN}\big(0, 1\big). \tag{35}$$

Then, let $\mathbf{h}_i^{\mathrm{NLoS}} = \tilde{\beta} \mathbf{z}_i$ with $\mathbf{z}_i \sim \mathcal{CN}(\mathbf{0}, \mathbf{I}_N)$ denote the i-th column of $\mathbf{H}_{\mathrm{NLoS}}$, when the number of N is large, the magnitude of diagonal entry in $\mathbf{G}_{\mathrm{NLoS}}$ approaches $N\mathbb{E}[\|\mathbf{h}_i^{\mathrm{NLoS}}\|^2] = \tilde{\beta}^2 N$ by the laws of large numbers, i.e., $|g_{ii}| \approx \tilde{\beta}^2 N$ [4]. Meanwhile, as for the (i, j)-th off-diagonal entry of $\mathbf{G}_{\mathrm{NLoS}}$, we have

$$|g_{ij}^{\mathrm{NLoS}}| = |(\mathbf{h}_i^{\mathrm{NLoS}})^{\mathrm{H}} \mathbf{h}_j^{\mathrm{NLoS}}| = \tilde{\beta}^2 |\mathbf{z}_i^{\mathrm{H}} \mathbf{z}_j|. \tag{36}$$

Accordingly, define $Z \triangleq \mathbf{z}_i^{\mathrm{H}} \mathbf{z}_j \in \mathbb{C}$ and express it as $Z = A + \mathrm{j}B$ with $A, B \in \mathbb{R}$. To consider the magnitude of the off-diagonal entry, we define

$$R = |Z| = |\mathbf{z}_i^{\mathrm{H}} \mathbf{z}_j| = \sqrt{A^2 + B^2}. \tag{37}$$

Next, we examine the statistical properties of R. First of all, by definition, the joint characteristic function (CF) of A and B is related to their joint probability density function (PDF) via a two-dimensional (2D) Fourier transform

$$\Psi_{A,B}(\omega_1, \omega_2) = 4\pi^2 \iint e^{\mathrm{j}(\omega_1 a + \omega_2 b)} f_{A,B}(a, b) \mathrm{d}a \mathrm{d}b. \tag{38}$$

In particular, for the inner product of two independent N-dimensional complex Gaussian random variables, the joint CF of the real and imaginary part, A and B, is given by [9]

$$\Psi_{A,B}(\omega_1, \omega_2) = \left(1 + \frac{\omega_1^2 + \omega_2^2}{4}\right)^{-N}. \tag{39}$$

Since $\Psi_{A,B}$ depends only on radial frequency $\rho = \sqrt{\omega_1^2 + \omega_2^2}$, the distribution of Z is spherical symmetric. In this case, the joint density in polar coordinates $f_{A,B}(r, \theta)$ depends only on the radial distribution $f_R(r)$,

$$f_R(r) = 2\pi r f_{A,B}(r, \theta), \tag{40}$$

where (f) holds because $f_{A,B}(r,\theta)$ is independent of θ under spherical symmetry. Meanwhile, the joint PDF $f_{A,B}(r,\theta)$ in (40) admits the representation [10]

$$f_{A,B}(r,\theta) \overset{(d)}{=} \frac{1}{4\pi^2}\int_0^{2\pi}\int_0^{\infty} e^{-\mathrm{j}\rho r\cos(\theta-\phi)}\Psi_{A,B}(\rho)\rho\mathrm{d}\rho\mathrm{d}\phi \overset{(e)}{=} \frac{1}{2\pi}\int_0^{\infty} J_0(\rho r)\Psi_{A,B}(\rho)\rho\mathrm{d}\rho, \tag{41}$$

where (d) stems from the 2D inverse Fourier transform of CF, (e) uses the integral identity of the zeroth-order Bessel function of the first kind, i.e., $2\pi J_0(\rho r)=\int_0^{2\pi} e^{-\mathrm{j}\rho r\cos(\theta-\phi)}\mathrm{d}\phi$.

Lemma 2. *The PDF of R $f_R(r)$ follows*

$$f_R(r)=\frac{4r^N}{\Gamma(N)}K_{N-1}(2r) \tag{42}$$

with the expectation given by

$$\mathbb{E}[R]=\frac{\sqrt{\pi N}}{2}, \tag{43}$$

where $\Gamma(\cdot)$ denotes the Gamma function and $K_\nu(\cdot)$ is the modified ν-order Bessel function of the second kind.

Proof: First of all, combining the spherical symmetry identities in (41) and (40), we arrive at the following expression for the radial density

$$f_R(r)=r\int_0^{\infty}\rho J_0(\rho r)\Big(1+\tfrac{\rho^2}{4}\Big)^{-N}\mathrm{d}\rho \overset{(g)}{=} \frac{4r^N}{\Gamma(N)}K_{N-1}(2r), \tag{44}$$

where (g) follows from the Bessel integral identity [11, Eq. (6.656.4)] with $\nu=0$, $\mu=N-1$, $a=2$, $b=r$, i.e.,

$$\int_0^{\infty}\frac{J_\nu(bx)\,x^{\nu+1}}{(x^2+a^2)^{\mu+1}}\,\mathrm{d}x=\frac{a^{\nu-\mu}b^\mu}{2^\mu\,\Gamma(\mu+1)}\,K_{\nu-\mu}(ab). \tag{45}$$

Then, based on $f_R(r)$ in (44), the mean of R follows

$$\mathbb{E}[R]=\int_0^{\infty} rf_R(r)\,\mathrm{d}r=\int_0^{\infty}\frac{4}{\Gamma(N)}r^{N+1}K_{N-1}(2r)\mathrm{d}r. \tag{46}$$

Moreover, according to [11, Eq. (6.562.16)], the following integral in terms of $K_\nu(z)$ can be reformulated as

$$\int_0^{\infty} x^\mu K_\nu(ax)\mathrm{d}x=2^{\mu-1}a^{-\mu-1}\Gamma(\tfrac{1+\mu+\nu}{2})\Gamma(\tfrac{1+\mu-\nu}{2}). \tag{47}$$

Next, with the substitution $x=r$, $\nu=N-1$, $\mu=N+1$, and $a=2$ in (47), the expression in (46) simplifies to

$$\mathbb{E}[R]=\frac{\sqrt{\pi}}{2}\frac{\Gamma\left(N+\frac{1}{2}\right)}{\Gamma(N)}. \tag{48}$$

After that, as $N\to\infty$, the Gamma ratio in (48) admits the Stirling's expansion, namely,

$$\frac{\Gamma(N+\frac{1}{2})}{\Gamma(N)}=\sqrt{N}\left(1-\frac{1}{8N}+\frac{1}{128N^2}+O(N^{-2})\right). \tag{49}$$

Therefore, substituting (49) into (48) concludes the proof. ∎

Corollary 2. *For $N,K\to\infty$ with $K/N<1$, by defining $G_i^{\mathrm{NLoS}}\triangleq\sum_{j\neq i}|g_{ij}^{\mathrm{NLoS}}|$, it follows that*

$$\mathbb{E}[G_i^{\mathrm{NLoS}}]\approx(K-1)\tilde{\beta}^2\frac{\sqrt{\pi N}}{2}. \tag{50}$$

Proof: First of all, Lemma 2 provides the expectation of radial distribution in (43). Based on it, the magnitude of off-diagonal g_{ij}^{NLoS} satisfies

$$\mathbb{E}[|g_{ij}^{\mathrm{NLoS}}|]=\tilde{\beta}^2\mathbb{E}[R]=\tilde{\beta}^2\frac{\sqrt{\pi N}}{2} \tag{51}$$

Moreover, since all off-diagonal magnitudes $|g_{ij}^{\mathrm{NLoS}}|$ are independent and identically distributed, G_i^{NLoS} follows

$$\mathbb{E}[G_i^{\mathrm{NLoS}}]=\mathbb{E}\big[\sum_{j\neq i}|g_{ij}^{\mathrm{NLoS}}|\big]=\sum_{j\neq i}\mathbb{E}\left[|g_{ij}^{\mathrm{NLoS}}|\right]. \tag{52}$$

Finally, substituting (51) into (52) completes the proof. ∎

C. Efficient Approximation of α^* by the Expectation of its Upper Bound

Based on the efficient approximations of both $\mathbf{G}_{\mathrm{LoS}}$ and $\mathbf{G}_{\mathrm{NLoS}}$, we now provide an efficient way to estimate the expectation of the upper bound of the proposed DDRI α^*, thus enabling the DDRI-based mechanism for XL-MIMO.

Typically, by letting $\bar{\alpha}$ denote the mean over α_is for $1\le i\le K$, i.e., $\bar{\alpha}=\frac{1}{K}\sum_{i=1}^K\alpha_i$, we have

$$\alpha^*\le\bar{\alpha}, \tag{53}$$

where Theorem 1 is given for the efficient approximation of $\bar{\alpha}$.

Theorem 1. *Given the channel model in* (2)*, for $N,K\to\infty$ with $K/N<1$, it follows that*

$$\mathbb{E}[\bar{\alpha}]\approx\frac{N}{N+\frac{\kappa}{\kappa+1}\left(\frac{2}{\pi\eta}\ln(NK\eta)+C\right)+\frac{1}{\kappa+1}\left(\frac{K-1}{2}\sqrt{\pi N}\right)}, \tag{54}$$

Proof: To start, the diagonal terms g_{ii} and the off-diagonal sums G_i concentrate around their expectations by the law of large numbers. Therefore,

$$\mathbb{E}[\bar{\alpha}]=\mathbb{E}\Big[\frac{|g_{ii}|}{|g_{ii}|+G_i}\Big]\approx\frac{\mathbb{E}[g_{ii}]}{\mathbb{E}[g_{ii}]+\mathbb{E}[G_i]}. \tag{55}$$

On one hand, the expected diagonal magnitude satisfies

$$\mathbb{E}[|g_{ii}|]=\frac{\kappa}{\kappa+1}|g_{ii}^{\mathrm{LoS}}|+\frac{1}{\kappa+1}\mathbb{E}[|g_{ii}^{\mathrm{NLoS}}|]=\tilde{\beta}^2N. \tag{56}$$

On the other hand, according to Lemma 1 and Corollary 2, we can obtain the approximation of the expectation of G_i as follows

$$\mathbb{E}[G_i]=\frac{\kappa}{\kappa+1}\sum_{j\neq i}|g_{ij}^{\mathrm{LoS}}|+\frac{1}{\kappa+1}\mathbb{E}\big[\sum_{j\neq i}|g_{ij}^{\mathrm{NLoS}}|\big] =\tilde{\beta}^2\big[\tfrac{\kappa}{\kappa+1}\big(\tfrac{2}{\pi\eta}\ln(NK\eta)+C\big)+\tfrac{1}{\kappa+1}\big(\tfrac{K-1}{2}\sqrt{\pi N}\big)\big], \tag{57}$$

Substituting (56) and (57) into (55) completes the proof. ∎

Based on Theorem 1, we propose to apply $\mathbb{E}[\bar{\alpha}]$ in (54) as an approximation of α^* to facilitate the DDRI-based judgement

mechanism. With this closed-form approximation, α^* can be roughly estimated with $\mathcal{O}(1)$ complexity, avoiding explicitly forming the Gram matrix or computing its spectrum. In fact, as shown in Fig. 4, the gap between α^* and $\mathbb{E}[\bar{\alpha}]$ is mild.

V. SIMULATION

In this section, simulation results are presented to validate the theoretical findings and provide further insights. We use the uplink detection scenario as a case study to demonstrate how the DDRI enables the judgement mechanism of signal processing strategies. Consider an XL-MIMO system operating at 30 GHz, corresponding to a wavelength of $\lambda = 0.01\ m$. Both transmitter and receiver are equipped with a ULA comprising $N = 1024$ antennas, with $K = 30$ antennas and a distance $r_0 = 100\ m$, thus ensuring near-field conditions. Pure NLoS, weak LoS, and strong LoS conditions are modeled by fixing the Rician K-factor to $\kappa = 0$, $\kappa = 4$ and $\kappa = 8$, respectively.

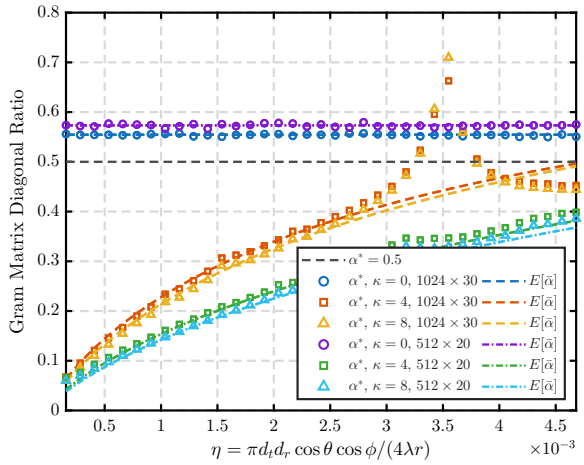

Fig. 4. Comparison of the real value of α^* in near-field and corresponding predicted value $\mathbb{E}[\bar{\alpha}]$ in (54) across Rician factors κ.

Fig. 4 plots the real value of DDRI α^* together with the corresponding predicted value $\mathbb{E}[\bar{\alpha}]$ derived in (54). The black dashed line indicates the threshold above which low-complexity methods are enabled. In the presence of a LoS component (i.e., $\kappa = 4$ and $\kappa = 8$) both the exact α^* and its approximation $\mathbb{E}[\bar{\alpha}]$ increase with the coupling parameter η regardless of the Rician-K factors. However, by setting $\kappa = 0$ in (54), we can obtain the expression for DDRI in pure NLoS condition. The resulting expression is then independent of coupling parameter η and is primarily determined by the system dimensions N and K. Additionally, a moderate-sized configuration with $N = 512$ and $K = 20$ is included to assess the effect of system dimensions, thereby demonstrating that $\mathbb{E}[\bar{\alpha}]$ remains stable across different array sizes.

It is also observed that, when a LoS component is present, Fig. 4 exhibits a surge around $\eta = 3.5 \times 10^{-3}$, which results from the zero point of (23). At this point, all off-diagonal interference terms tend to zero, thus producing an extremely large value of the DDRI.

Fig. 5 compares the BER performance under different DDRI levels. As α^* increases, the channel quality becomes better conditioned, leading to a consistent improvement in the detection performance of the conventional MMSE scheme. Meanwhile, the performance gap between MMSE method and the low-complexity conjugate gradient (CG) detector narrows consistently. In particular, when $\alpha^* \geq 0.5$, the CG curve nearly coincides with the MMSE curve across the entire range considered.

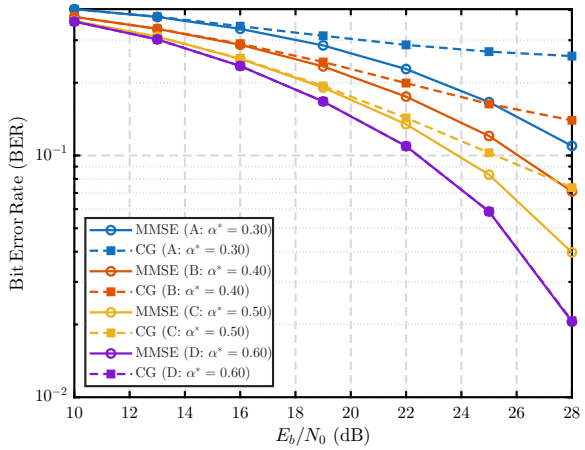

Fig. 5. Near-field BER comparison for MMSE and Low-Complexity Methods (CG) under different DDRI α^* levels, i.e., $\alpha^* \in \{0.30, 0.40, 0.50, 0.60\}$.

ACKNOWLEDGMENT

This work was supported in part by the National Key R&D Program of China under Grants No.2023YFC2205501, in part by National Science and Technology Major Projects of China under Grant 2025ZD1301800, and in part by National Natural Science Foundation of China under Grants No.62371124.

REFERENCES

[1] Y. Liu, Z. Wang, J. Xu, C. Ouyang, X. Mu, and R. Schober, "Near-field communications: A tutorial review," *IEEE Open J. Commun. Soc.*, vol. 4, pp. 1999–2049, 2023.

[2] H. Lu, Y. Zeng, C. You, Y. Han, J. Zhang, Z. Wang, Z. Dong, S. Jin, C.-X. Wang, T. Jiang *et al.*, "A tutorial on near-field XL-MIMO communications toward 6G," *IEEE Commun. Surv. Tutorials*, vol. 26, no. 4, pp. 2213–2257, 2024.

[3] J. Tian, Y. Han, S. Jin, J. Zhang, and J. Wang, "Analytical channel modeling: From MIMO to extra large-scale MIMO," *Chinese J. Elect.*, vol. 34, no. 1, pp. 1–15, Jan. 2025.

[4] D. Zhu, B. Li, and P. Liang, "On the matrix inversion approximation based on Neumann series in massive MIMO systems," in *Proc. IEEE Int. Conf. Commun.*, London, U.K., 2015, pp. 1763–1769.

[5] Z. Wang, R. M. Gower, Y. Xia, L. He, and Y. Huang, "Randomized iterative methods for low-complexity large-scale MIMO detection," *IEEE Trans. Signal Process.*, vol. 70, pp. 2934–2949, 2022.

[6] J. Liu, Y. Ma, and R. Tafazolli, "A spatially non-stationary fading channel model for simulation and (semi-) analytical study of ELAA-MIMO," *IEEE Trans. Wireless Commun.*, vol. 23, no. 5, pp. 5203–5218, 2023.

[7] X. Chen, H. Ren, C. Pan, Z. Peng, and J. Wang, "What is the optimal antenna spacing from the perspective of effective DoF for XL-MIMO systems?" *IEEE Wireless Commun. Lett.*, 2025.

[8] R. A. Horn and C. R. Johnson, *Matrix Analysis*, 2nd ed. Cambridge, U.K.: Cambridge University Press, 2012.

[9] R. K. Mallik and N. C. Sagias, "Distribution of inner product of complex gaussian random vectors and its applications," *IEEE Trans. Commun.*, vol. 59, no. 12, pp. 3353–3362, 2011.

[10] L. Huang and T. C. Chong, "Channel modeling and target design for two-dimensional optical storage systems," *IEEE Trans. Magn.*, vol. 41, no. 8, pp. 2414–2424, 2005.

[11] I. S. Gradshteyn and I. M. Ryzhik, *Table of integrals, series, and products*, 8th ed. Academic Press, 2014.